

Foam-Filled Grooved Tubes with Circular Cross-Section Under Axial Compression: A Theoretical Analysis

Abbas Niknejad¹ · Mohammad Mahdi Abedi¹ · Gholam Hossein Liaghat² · Mohammad Zamani Nejad¹

Received: 31 January 2016 / Accepted: 8 July 2016 / Published online: 15 July 2016
© Shiraz University 2016

Abstract In this article, some theoretical relations are derived to predict the instantaneous folding force and the absorbed energy by the empty and polyurethane foam-filled grooved tubes with circular cross-section during the first fold formation under the axial loading. Five different modes of deformation are considered in the theoretical model of deformation: bending around two internal circular hinge lines, bending around an external circular hinge line, extensional deformation in the folding arms, axial compression of the polyurethane foam, and interaction effects between polyurethane foam and inner wall of the grooved tube. Also, based on the experiments, a semi-empirical relation is suggested to predict the effective axial displacement at the end of a complete fold creation in the polyurethane foam-filled grooved tubes. To verify the theoretical analyses, some axial compression tests were carried out on the empty and filled grooved tubes. Comparison of the theoretical predictions with the corresponding experimental results showed a good correlation.

Keywords Axial compression · Energy method · Folding · Grooved tube · Polyurethane foam

1 Introduction

The survivability of the driver in an accident is achieved by a combination of the crash resistance of the car and its ability to absorb energy. This has been achieved by providing a survival cell (the chassis), which is extremely resistant to damage, around which energy absorbing devices are placed at strategic points on the vehicle. The energy absorbing devices operate to enable maximum deformation up to a specified limit. The devices used are designed to dissipate energy irreversibly during the impact, thereby reducing the force and momentum transferred to the survival cell and hence the driver (Savage et al. 2004). Tubular thin-walled structures with different shapes of sections are widely used in various transportation systems as energy absorbing components to dissipate the kinetic energy during accidents of collision and crash. To design these structures with less weight and excellent crashworthiness, performance is a significant task for the sake of public safety, energy saving, and environmental protection (Zhang and Huh 2009). Filling tubular structures with appropriate lightweight materials such as foam (Wang et al. 2011; Tan et al. 2005) or honeycomb materials (Nakamoto et al. 2009; Zou et al. 2009) are one of the options to improve the energy absorption characteristics.

Circular or square sectioned tubes are one of the most commonly used structural elements due to their prevalent occurrence and easy manufacturability (Niknejad et al. 2012). Niknejad (2010) introduced a theory to estimate the instantaneous folding force of the first fold creation in the square and rectangular columns and then investigated the effects of polyurethane foam-filler on the folding behavior of the square columns by theoretical and experimental methods (Niknejad et al. 2011). Bardi et al. (2003) presented a combined experimental analytical study of the

✉ Abbas Niknejad
Aniknejad@yu.ac.ir

¹ Mechanical Engineering Department, Yasouj University,
P.O. Box: 75914-353, Yasouj, Iran

² Mechanical Engineering Department, Tarbiat Modares
University, P.O. Box: 14115-143, Tehran, Iran

onset of collapse, its localization and the subsequent progressive folding in the empty circular tubes made of different metal alloys. Tyagi et al. (2004) developed a partly inside and partly outside curved fold model with variable straight length and stepped variation in the thickness of circular tube during folding process. All model parameters videlicet size of fold, optimal value of folding parameter, maximum hinge angle, and the final radius of curvature of fold were evaluated analytically (Tyagi et al. 2004).

Tasdemirci (2008) studied the effect of various types of end constraining on the deformation and load–displacement behavior of a 3003-H14 Al tube, experimentally and numerically. Bardi and Kyriakides (2006) presented the results of an experimental study involving stainless steel specimens with different diameter-to-thickness ratios. Specimens were subsequently compressed to failure under displacement control, and the evolution of wrinkles was monitored using a special surface-scanning device (Bardi and Kyriakides 2006).

Metal foams exhibit unusual mechanical properties not found in solid materials. In particular, the energy absorbed during deformation of metal foam can be extremely high, a phenomenon that stems from the mechanisms of cell wall collapse (Park and Nutt 2002). Guden and Kavi (2006) investigated the axial crushing behavior of empty and Al close-cell foam-filled single Al tubes and Al multi-tube designs (hexagonal and square) through quasi-static compression testing. The effects of foam filling on the deformation mode and the crushing and average crushing loads of single tubes and multi-tube designs were determined, experimentally. It was found that the aluminum foam filling induced a higher strengthening coefficient in multi-tube than single tubes and increased the energy absorption in single tubes and multi-tube designs (Guden and Kavi 2006). Lee et al. (2008) manufactured an energy absorption controller, a control tool to increase proper deformation and energy absorption capability, and compared and examined the effect of controller usage on energy absorption capability for the Al thin-walled tube member, in order to obtain design data for the vehicle structural member that has the most efficient energy absorption performance. Adachi et al. (2008) performed experimental and theoretical analyses that show a thin-walled cylinder with stiff ribs can be used as a structural element to improve or adjust energy absorption characteristics. They conducted impact crushing tests using several different cylinders with ribs and showed that the axisymmetric and non-axisymmetric crushing modes are dependent on not only the cross-section size but also on the distances between the ribs (Adachi et al. 2008). Li et al. (2012) carried out some experiments to investigate the deformation and energy absorption characteristics of aluminum foam-filled double tubes subjected to oblique loading. A test rig was designed and

manufactured to perform the quasi-static oblique loading experiments on three types of tubular structures: Empty, foam-filled single and double tubes, and their energy absorption characteristics with respect to the load angle and wall thickness were determined and compared (Li et al. 2012). Abedi et al. (2012), Niknejad et al. (2015) drove some theoretical relations to predict diagrams of absorbed energy and axial force versus axial displacement during the folding process in square and rectangular columns. By considering the folding wavelength as a constant parameter during the folds creation and using balance of internal and external energy and minimum principle in plasticity, final relations were calculated. Niknejad and Tavassolimanesh (2013) and Niknejad et al. (2013) presented different plastic deformations like curling, inversion (Niknejad and Tavassolimanesh 2013) and splitting (Niknejad et al. 2013) on circular cross-sectional areas and produced new theoretical models during the plastic deformations. They could compare experimental results with theoretical analyses to predict the crushing load and energy absorption capacity of these structures. Crashworthiness characteristics of thin-walled steel tubes containing annular grooves were experimentally studied by Hosseini-pour and Daneshi (2002). Niknejad et al. (2012) investigated the effects of grooves on the mean buckling load of polyurethane foam-filled tubes with circular cross-section under axial compression. They derived some theoretical relations to predict the mean folding force, total absorbed energy per unit of tube length, and specific absorbed energy per unit of total mass by the polyurethane foam-filled grooved tubes with circular cross-section under the axial compression process. Also, during the folding process, a new theoretical model of deformation was introduced for the polyurethane foam-filler (Niknejad et al. 2012).

In some practices, such as columns or supports of bumper cross-beam of automotives, axial compression loads are applied on thin-walled specimens. Depending on crash direction, sometimes there is a certain angle between direction of applied load and axis of thin-walled specimens. Folding of thin-walled sections is a plastic deformation mechanism that has very high ratio of absorbed energy per mass, respect to some other energy absorption mechanisms such as lateral flattening. When lateral surfaces of a thin-walled tube are machined, some circumferential grooves are created on the surfaces and a thin-walled grooved tube is produced. When axial load or even inclined load is applied on a grooved tube, probability of creation of the regular folds in the tube wall increases and consequently, probability of higher energy absorption capacity may enhances. Also, the empty space inside thin-walled specimens can be used by injecting the porous materials such as aluminum or polyurethane foam. As an application, thin-walled grooved tubes can be used as the supports

(columns) of bumper cross-beam of the automotives. Reviewing of the published works shows that average value of folding force in the circular grooved tubes was calculated, previously. In this article, some theoretical formulas are derived to predict instantaneous folding force and absorbed energy by the circular grooved tubes in two conditions: empty and polyurethane foam-filled. Then, some axial compression tests are performed on the empty and filled circular brazen tubes to verify the presented theories.

2 Theoretical analysis

Geometrical dimensions of an empty grooved tube with circular cross-section are shown in Fig. 1. In the theoretical analysis, the following assumptions are considered:

- The friction between tube and steel platens is neglected.
- Mechanical behavior of the tubes material is considered as rigid-perfectly plastic, and therefore, the elastic strain and the strain hardening in plastic hinges are neglected.
- The relation between stress and strain obeys equation $\sigma = k\epsilon^n$, where, k and n indicate the strength coefficient and the strain hardening exponent, respectively.
- The volume of the tube material remains constant, during the axial compression.
- The Poisson’ ratio of the polyurethane foam is zero.

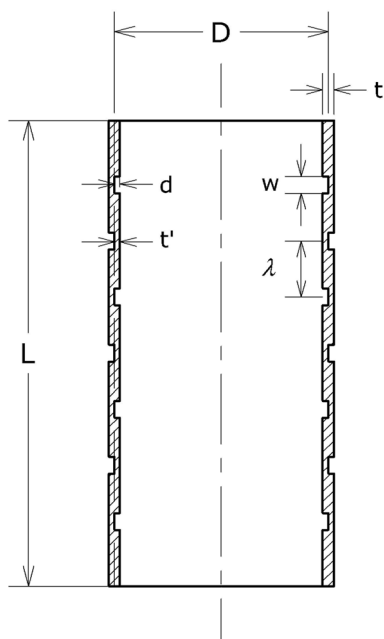


Fig. 1 Geometrical characteristics of circular grooved tube

Figure 2 shows a foam-filled grooved tube with the circular cross-section before and after the first fold creation and the theoretical model of deformation. According to the figure, a part of the grooved tube with the initial length of 2λ is considered as the unit element of deformation and called basic folding element (BFE). The axial displacement that called instantaneous folding distance designated by δ indicates the decrement of axial distance between the upper and lower edges of the BFE. According to Fig. 2, this quantity is calculated as:

$$\delta = 2\lambda(1 - \cos \alpha) \tag{1}$$

In the above equation, λ and α are grooves distance and folding angle, respectively. Differentiating the above equation results in the axial displacement rate versus the folding angle rate $\dot{\alpha}$, as the following relation:

$$\dot{\delta} = 2\lambda \cdot \sin \alpha \cdot \dot{\alpha} \tag{2}$$

According to the theoretical deformation model (BFE) in Fig. 2, five different modes of deformation are considered during a fold creation in the foam-filled grooved tubes:

- Bending around circular hinge lines A and C.
- Bending around circular hinge line B.
- Extensional deformation in the folding arms AB and BC.
- Axial compression of the polyurethane foam.
- Interaction effects between polyurethane foam and inner wall of the grooved tube (The analysis is performed in two different conditions: without and with considering the interaction effects).

Summation of the dissipated bending energy rates in the two circular hinge lines A and C during a fold creation is obtained as:

$$\dot{E}_{A,C} = \dot{E}_A + \dot{E}_C = 2M_0\pi D\dot{\alpha} \tag{3}$$

In the above equation, D is mean diameter of circular grooved tube and M_0 is the perfectly plastic bending moment and obtained as (Daneshi and Hosseinipour 2002):

$$M_0 = \frac{2}{\sqrt{3}} \sigma_0 \frac{t'^2}{4} \tag{4}$$

where σ_0 is flow stress of tube material and t' is tube wall thickness in grooves.

Rate of the dissipated energy by bending around circular hinge line B during a fold creation is calculated as following:

$$\dot{E}_B = M_0\pi(D + 2\lambda \sin \alpha)2\dot{\alpha} \tag{5}$$

Therefore, the total energy rate by bending around the circumferential groove lines of a BFE during a fold creation designated by \dot{E}_b is obtained as:

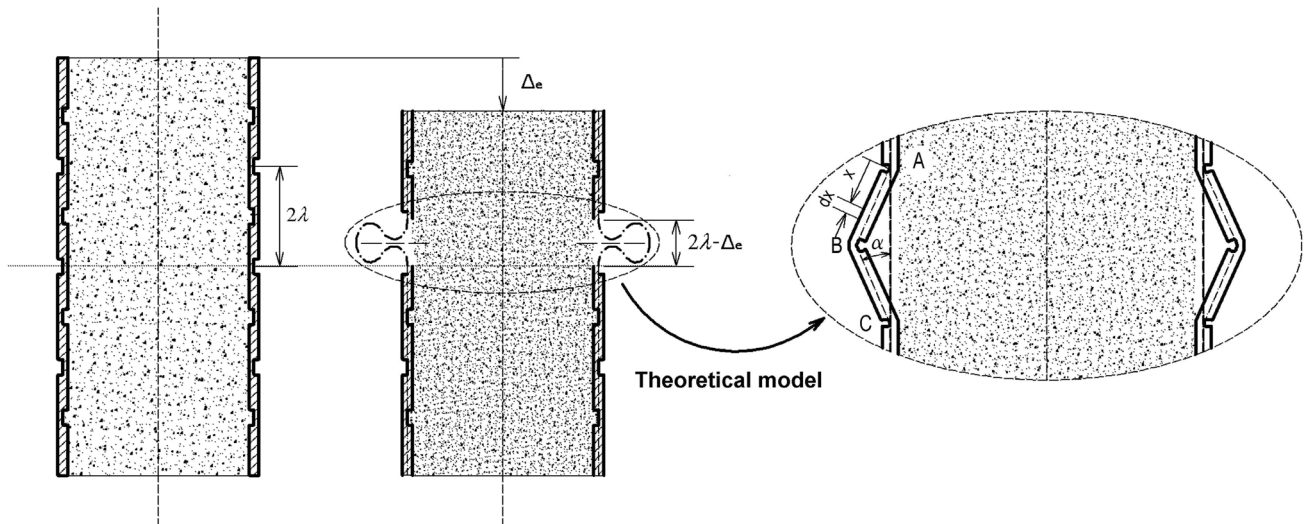


Fig. 2 Circular grooved tube before and after the first fold creation and the theoretical model

$$\dot{E}_b = \dot{E}_{A,C} + \dot{E}_B = \frac{2}{\sqrt{3}} \pi \sigma_0 t'^2 (D + \lambda \sin \alpha) \dot{\alpha} \quad (6)$$

Now, the dissipated energy rate by the extensional deformation in the folding arms is calculated, based on the strain energy relation as below:

$$dE_{ex} = \sigma_0 \varepsilon dV \quad (7)$$

where V is volume of the deformed material. The flow stress of the tube material is estimated by the following formula (Santosa et al. 2000):

$$\sigma_0 = \sqrt{\frac{\sigma_y \sigma_u}{1+n}} \quad (8)$$

In the above relation, σ_y , σ_u , and n are yield stress, ultimate stress, and strain hardening exponent of the tube material, respectively.

The circumferential strain due to extensional mode in the folding arms AB and BC is obtained as:

$$\varepsilon_{ex} = \frac{2x \sin \alpha}{D} \quad (9)$$

Figure 2 shows the mentioned quantities in the above equation. By substituting the extensional strain from (9) in (7) and integrating all over a BFE and dividing height of a BFE to three different parts with the wall thickness of t' , t , and t' , respectively, the following relation is resulted in:

$$E_{ex} = 2\sigma_0 \left[\int_0^{\frac{w}{2}} \pi D t' \frac{2x \sin \alpha}{D} dx + \int_{\frac{w}{2}}^{\lambda - \frac{w}{2}} \pi D t \frac{2x \sin \alpha}{D} dx + \int_{\lambda - \frac{w}{2}}^{\lambda} \pi D t' \frac{2x \sin \alpha}{D} dx \right] \quad (10)$$

In the above relation, width of grooves indicated by w . It is considered that t' and t remain constant during the

deformation process. According to the theoretical deformation model of grooved tubes (Fig. 2), during a fold creation, the tube wall moves outward, and consequently, circumferential extension occurs in the tube wall. During the hoop extension of the tube wall, axial compression load is applied on the tube wall, too. Therefore, thinning of the tube wall due to the hoop extension compensates by decreasing the tube length due to the axial compression load. However, decrement of tube length is very small and can be neglected. According to the recent justification, in the theoretical model, it is considered that during the folding process tube wall thickness remains constant.

Therefore, the dissipated energy by the extensional deformation in a grooved tube is derived as:

$$E_{ex} = 2\pi \sigma_0 \sin \alpha (t\lambda^2 - t\lambda w + t'\lambda w) \quad (11)$$

Differentiating the above relation results in the dissipated energy rate of the extensional deformation in the folding arms of a BFE:

$$\dot{E}_{ex} = 2\pi \sigma_0 \cos \alpha (t\lambda^2 - t\lambda w + t'\lambda w) \dot{\alpha} \quad (12)$$

Therefore, the total dissipated energy rate by a circular grooved tube during a fold creation is obtained as following:

$$\dot{E}_{BFE} = 2\pi \sigma_0 \left[\frac{t'^2}{\sqrt{3}} (D + \lambda \sin \alpha) + \cos \alpha (t\lambda^2 - t\lambda w + t'\lambda w) \right] \dot{\alpha} \quad (13)$$

2.1 Instantaneous Folding Force of the Empty Grooved Tube

Rate of the performed work by the external load on a circular grooved tube under the axial loading during a fold creation is calculated as:

$$\dot{W}_{ext} = P \dot{\delta} = P \cdot 2\lambda \sin \alpha \cdot \dot{\alpha} \quad (14)$$

The required external work rate for compressing a circular grooved tube is equated with the internal dissipated energy rate. Therefore, the following relation is derived by equating (13) and (14):

$$P = \pi\sigma_0 \left[\frac{t'^2}{\sqrt{3}} \left(\frac{D}{\lambda \sin \alpha} + 1 \right) + \cot \alpha (t\lambda - tw + t'w) \right] \quad (15)$$

The above formula predicts the instantaneous axial force of the circular grooved tube versus the folding angle α . By calculating the axial displacement δ from (1) and substituting in the above relation, the final formula is derived as:

$$P = \pi\sigma_0 \left[\frac{t'^2}{\sqrt{3}} \left(\frac{D}{\lambda \sqrt{\frac{\delta}{\lambda} \left(1 - \frac{\delta}{4\lambda} \right)}} + 1 \right) + \frac{1 - \frac{\delta}{2\lambda}}{\sqrt{\frac{\delta}{\lambda} \left(1 - \frac{\delta}{4\lambda} \right)}} (t\lambda - tw + t'w) \right] \quad (16)$$

Equation (16) predicts diagram of axial force versus the axial displacement during the first fold creation in a circular grooved tube, theoretically.

2.2 Absorbed Energy by the Empty Grooved Tube

Integration of (13) results in the absorbed energy by the empty grooved tube with circular cross-section versus the folding angle:

$$E = 2\pi\sigma_0 \left[\frac{t'^2}{\sqrt{3}} (D \cdot \alpha + \lambda - \lambda \cos \alpha) + \sin \alpha (t\lambda^2 - t\lambda w + t'\lambda w) \right] \quad (17)$$

By substituting the axial displacement δ from (1) in the above relation, the following relation is derived to estimate diagram of the absorbed energy by the empty grooved tube versus the axial displacement during a fold formation:

$$E = 2\pi\sigma_0 \left[\frac{t'^2}{\sqrt{3}} \left(D \cos^{-1} \left(1 - \frac{\delta}{2\lambda} \right) + \lambda - \lambda \left(1 - \frac{\delta}{2\lambda} \right) \right) + \sqrt{\frac{\delta}{\lambda} \left(1 - \frac{\delta}{4\lambda} \right)} (t\lambda^2 - t\lambda w + t'\lambda w) \right] \quad (18)$$

2.3 Instantaneous Folding Force of the Foam-Filled Grooved Tube

The initial volume of the polyurethane foam-filler is obtained as:

$$V_1 = \lambda\pi \frac{(D-t)^2}{2} + \pi(D-d)dw \quad (19)$$

Secondary volume of the polyurethane foam during a fold creation in the filled circular grooved tube is calculated as following:

$$V_2 = \lambda\pi \frac{(D-t)^2}{2} \cos \alpha \quad (20)$$

Therefore, the dissipated energy rate by the polyurethane foam is derived as:

$$\dot{E}_f = \sigma_p \cdot \Delta \dot{V} = \frac{\pi}{2} \sigma_p \lambda (D-t)^2 \cdot \sin \alpha \cdot \dot{\alpha} \quad (21)$$

In the above relation, σ_p indicates plateau stress of the polyurethane foam and $\Delta \dot{V}$ is volume variation rate of the foam. Summation of the dissipated energy rates by the polyurethane foam and a BFE results in total dissipated energy rate by a filled grooved tube:

$$\dot{E}_{tot} = \left[\frac{2\pi\sigma_0 t'^2}{\sqrt{3}} (D + \lambda \sin \alpha) + 2\pi\sigma_0 \cdot \cos \alpha (t\lambda^2 - t\lambda w + t'\lambda w) + \frac{\pi}{2} \sigma_p \lambda (D-t)^2 \cdot \sin \alpha \right] \dot{\alpha} \quad (22)$$

Dividing the total dissipated energy rate by a filled grooved tube to the axial displacement rate is results in the following relation:

$$P = \left[\frac{\pi\sigma_0 t'^2}{\sqrt{3}} \left(\frac{D}{\lambda \sin \alpha} + 1 \right) + \pi\sigma_0 \cdot \cot \alpha (t\lambda - tw + t'w) + \frac{\pi}{4} \sigma_p (D-t)^2 \right] \quad (23)$$

Substituting the folding angle α versus the axial displacement from (1) in (23) results in the following relation:

$$P = \pi\sigma_0 \left[\frac{t'^2}{\sqrt{3}} \left(\frac{D}{\lambda \sqrt{\frac{\delta}{\lambda} \left(1 - \frac{\delta}{4\lambda} \right)}} + 1 \right) + \frac{1 - \frac{\delta}{2\lambda}}{\sqrt{\frac{\delta}{\lambda} \left(1 - \frac{\delta}{4\lambda} \right)}} (t\lambda - tw + t'w) \right] + \frac{\pi}{4} \sigma_p (D-t)^2 \quad (24)$$

Equation (24) predicts the instantaneous folding force of the polyurethane foam-filled grooved tube versus the axial displacement without considering the interaction effects. Niknejad et al. (2012) investigated the interaction effects between polyurethane foam and inner wall of the circular grooved tube on the mean absorbed energy by the structure during the axial compression. In (Niknejad et al. 2012), by experimental measurements of the mean absorbed energy in the filled grooved tubes, they calculated the interaction factor equal to 2. On the other hand, they showed the absorbed energy due to the interaction effects is equal to the absorbed energy by the polyurethane foam. Therefore, the following relation estimates diagram of the instantaneous folding force versus the axial displacement with considering the interaction effects between polyurethane foam and inner wall of the tube, theoretically:

$$P = \pi\sigma_0 \left[\frac{t^2}{\sqrt{3}} \left(\frac{D}{\lambda\sqrt{\frac{\delta}{\lambda}\left(1-\frac{\delta}{4\lambda}\right)} + 1} \right) + \frac{1-\frac{\delta}{2\lambda}}{\sqrt{\frac{\delta}{\lambda}\left(1-\frac{\delta}{4\lambda}\right)}} (t\lambda - tw + t'w) \right] + \frac{\pi}{2}\sigma_p(D-t)^2 \quad (25)$$

2.4 Absorbed Energy by the Filled Grooved Tube

Equation (22) predicts the total dissipated energy rate by a filled grooved tube versus the folding angle without considering the interaction effect. Integrating (22) results in the total dissipated energy by a foam-filled grooved tube versus the folding angle as the following relation:

$$E = 2\pi\sigma_0 \left[\frac{t^2}{\sqrt{3}} (D \cdot \alpha + \lambda - \lambda \cos \alpha) + \sin \alpha (t\lambda^2 - t\lambda w + t'\lambda w) \right] + \frac{\pi}{2}\sigma_p\lambda(D-t)^2(1 - \cos \alpha) \quad (26)$$

Therefore, the following relation is derived to predict diagram of the absorbed energy by a filled circular grooved tube versus the axial displacement during a fold creation under the axial loading without considering the interaction effects between polyurethane foam and inner wall of the tube, theoretically:

$$E = 2\pi\sigma_0 \left[\frac{t^2}{\sqrt{3}} \left(D \cos^{-1} \left(1 - \frac{\delta}{2\lambda} \right) + \lambda - \lambda \left(1 - \frac{\delta}{2\lambda} \right) \right) + \sqrt{\frac{\delta}{\lambda} \left(1 - \frac{\delta}{4\lambda} \right)} (t\lambda^2 - t\lambda w + t'\lambda w) \right] + \frac{\pi}{4}\sigma_p(D-t)^2 \cdot \delta \quad (27)$$

Finally, the following relation calculates the absorbed energy by the filled grooved tube versus the axial displacement during the axial compression with considering the interaction effects:

$$E = 2\pi\sigma_0 \left[\frac{t^2}{\sqrt{3}} \left(D \cos^{-1} \left(1 - \frac{\delta}{2\lambda} \right) + \lambda - \lambda \left(1 - \frac{\delta}{2\lambda} \right) \right) + \sqrt{\frac{\delta}{\lambda} \left(1 - \frac{\delta}{4\lambda} \right)} (t\lambda^2 - t\lambda w + t'\lambda w) \right] + \frac{\pi}{2}\sigma_p(D-t)^2 \cdot \delta \quad (28)$$

Also, Niknejad et al. (2012) showed that the effective folding distance (effective axial displacement) of the polyurethane foam-filled grooved tube designated by Δ_e obeys the following relation:

$$\Delta_e = 1.72\lambda - t \quad (29)$$

Δ_e is shown in Fig. 2 and indicates the final displacement of the tube after a fold formation. Substituting the

effective folding distance from the above equation to (1) results in:

$$\alpha_f = \cos^{-1} \left(0.14 + \frac{t}{2\lambda} \right) \quad (30)$$

where α_f indicates final value of the folding angle, after creating a complete fold in the circular grooved tube.

3 Experiments

Some seamless circular brazen tubes were prepared as the axial compression test specimens. The tubes were machined, and annular grooves were cut alternately inside and outside the tube surfaces. The depth of grooves in all specimens is one half of the tube's wall thickness, and the width of grooves is 3 mm. To achieve symmetry of deformation, the numbers of grooves are chosen to be odd and the first groove is inside the tube wall. The lengths of the specimens are chosen to be proportional to the distances between the grooves. Characteristics of the empty specimens are given in Table 1. Quasi-static axial compression tests were performed by a DMG hydraulic testing machine at a nominal cross-head speed of 5 mm/min. The specimens were crushed between parallel steel platens of the test machine without any additional fixing, and diagram of the axial load versus the axial displacement were plotted for each test and then experimental absorbed energy was calculated by measuring the area under the load–displacement curve. The specimens vary in the distance between the grooves, number of grooves, the tube length, and type of polyurethane foam-filler.

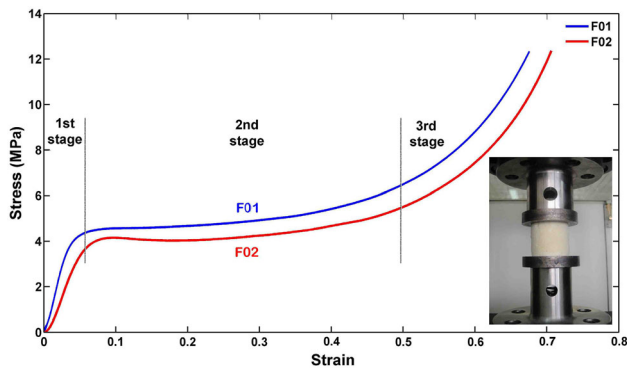
Two types of polyurethane foam were used to prepare the foam-filled circular grooved tubes. Table 2 gives characteristics of the filled specimens. To determine material properties of the polyurethane foam, a solid cylindrical specimen of each type of polyurethane foams was prepared and axially compressed. Figure 3 illustrates compressive stress–strain diagram of two types of polyurethane foam. Cellular solids such as polyurethane foams are made up of interconnected networks of solid struts or plates that form the edges and faces of cells. According to Fig. 3, diagram of axial compressive stress of the polyurethane foams versus axial strain is divided to three stages. Firstly, at small strains, by increasing the axial strain, axial stress increases linearly, due to the bending of cells wall. In the second stage, there is a large increment in the axial strain without a considerable increment in the axial load and it is due the elastic–plastic buckling of the columns and plates that make up the cells edge and wall. Therefore, in the second stage, the stress–strain curve transforms to a horizontal line. In the third stage, the compressive stress on the polyurethane foam rises rapidly

Table 1 Geometrical dimensions of the empty grooved tubes

Empty specimens code	L (mm)	D (mm)	t (mm)	t' (mm)	d (mm)	w (mm)	λ (mm)
GT1	48	48.2	1.8	0.9	0.9	3	12
GT2	44	48.2	1.8	0.9	0.9	3	11
GT3	54	48.2	1.8	0.9	0.9	3	9
GT4	48	48.2	1.8	0.9	0.9	3	8
GT5	42	48.2	1.8	0.9	0.9	3	7

Table 2 Geometrical dimensions of the foam-filled grooved tubes and type of polyurethane foam-fillers

Filled specimens code	Foam type	L (mm)	D (mm)	t (mm)	t' (mm)	d (mm)	w (mm)	λ (mm)
FGT1	Foam2	88	48.2	1.8	0.9	0.9	3	11
FGT2	Foam1	80	48.2	1.8	0.9	0.9	3	8
FGT3	Foam2	70	48.2	1.8	0.9	0.9	3	7
FGT4	Foam1	70	48.2	1.8	0.9	0.9	3	7
FGT5	Foam2	60	48.2	1.8	0.9	0.9	3	6

**Fig. 3** The compressive stress–strain diagram of the polyurethane foams

after the foam densification, while, the cell walls crush together. To consider influences of the densification stage of the foam on energy absorption of the structure, mean compressive stress of each type of polyurethane foams was considered as the plateau stress. The proposed theoretical relations have been derived to predict instantaneous folding force and energy absorption of polyurethane foam-filled grooved tubes during the first fold creation. In this case (first fold creation), cells wall of porous polyurethane foam do not crush together; consequently, mechanical compression of the polyurethane foam occurs through the second stage. Therefore, in the theory, mechanical behavior of the polyurethane foam was modeled as the rigid-perfectly plastic with constant plateau stress. Table 3 gives material properties of the polyurethane foams. To determine material properties of the tubes material, a dumbbell shape specimen of the tubes material was made and a

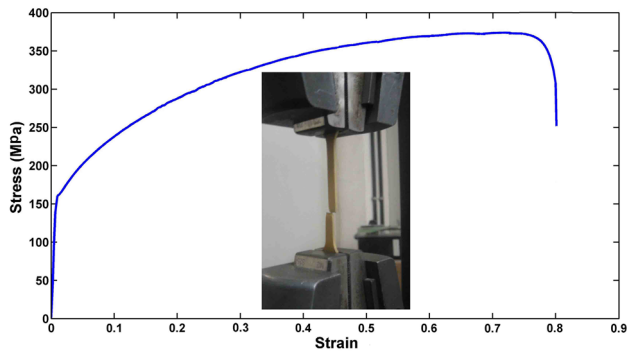
quasi-static tension test was carried out according to ASTM E8M. Tensile stress–strain diagram of the tube material has been sketched in Fig. 4. Brass alloy is a ductile material, therefore, when axial load is applied on the dumbbell shape brazen sample; according to Fig. 4, firstly, its length increases intensively, till the applied stress reaches to the yield strength. Then, due to the slippage of the material along oblique surfaces, large deformations occur through the work hardening progress. After the yield strength, elongation of the specimen can be several times of its elastic deformations. During the plastic deformations, due to the work hardening, strain hardening exponent of the alloy is between 0 and 1; so, effect of the work hardening has been considered in the theoretical relation (8). After a certain maximum value of the load (ultimate strength) has been reached, the surface of a portion of the specimen begins to decrease, because of local instability. Table 4 gives properties of the grooved tubes material. Figures 5 and 6 show some empty and foam-filled specimens before the tests, respectively.

4 Results and Discussion

In this article, theoretical relations (16) and (18) were derived to predict the instantaneous folding force and the absorbed energy by an empty grooved tube during the first fold creation, respectively. Also, theoretical formulas (24) and (25) estimate the instantaneous folding force of the filled specimens, respectively, without and with considering the interaction effect. Furthermore, analytical relations (27) and (28) were calculated to predict the absorbed energy by a polyurethane foam-filled grooved tube,

Table 3 Material properties of the polyurethane foams

Foam code	Density (kg/m ³)	Modulus of elasticity (GPa)	Plateau stress (MPa)
Foam 1	244	1.161	4.8
Foam 2	222	0.802	4.3

**Fig. 4** Tensile stress–strain diagram of the dumbbell shape specimen of the brazen tube

respectively, without and with considering the interaction effect between inner wall of the tube and lateral surface of polyurethane foam. To verify the presented theories, the experimental measurements are compared with the corresponding theoretical predictions.

4.1 Verification of Equation (16)

Figures 7, 8, 9, 10, and 11 show comparison of the theoretical predictions with the corresponding experimental

results of the instantaneous folding force of the empty specimens versus the axial displacement during the first fold creation. The figures show that the analytical relation (16) estimates diagram of axial load–displacement of the empty grooved tube with a reasonable correlation. Also, comparison of the slope of the theoretical and experimental curves shows that the theoretical relation calculates the folding force variation with a good correlation and it is affirmed verity of general form of the mathematical function in Eq. (16). Also, images of the specimens after the axial compression tests show that the grooves creation in the circular metal tubes constrains plastic deformation of the specimen and causes formation of the circumferential plastic hinge ring in the grooves of the specimen.

4.2 Verification of Equation (18)

Figures 12 and 13 compare theoretical and experimental diagram of the absorbed energy by empty grooved tubes during the first fold creation. According to the figures it is results in although, there is a difference between the theoretical predictions and the experiments, Eq. (18) calculates the general form of the curve with good correlation. In derivation of Eq. (18), three different deformation modes

Table 4 Material properties of the grooved tubes

Material type	Density (kg/m ³)	Modulus of elasticity (GPa)	Yield stress (MPa)	Ultimate stress (MPa)	Strain hardening exponent	Flow stress (MPa)
Brass alloy	8700	110	160	376	0.24	220.26

**Fig. 5** Empty circular grooved tubes before the tests

Fig. 6 Polyurethane foam-filled circular grooved tubes before the tests

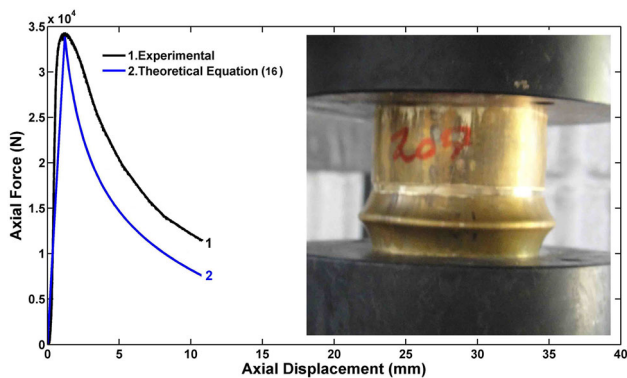
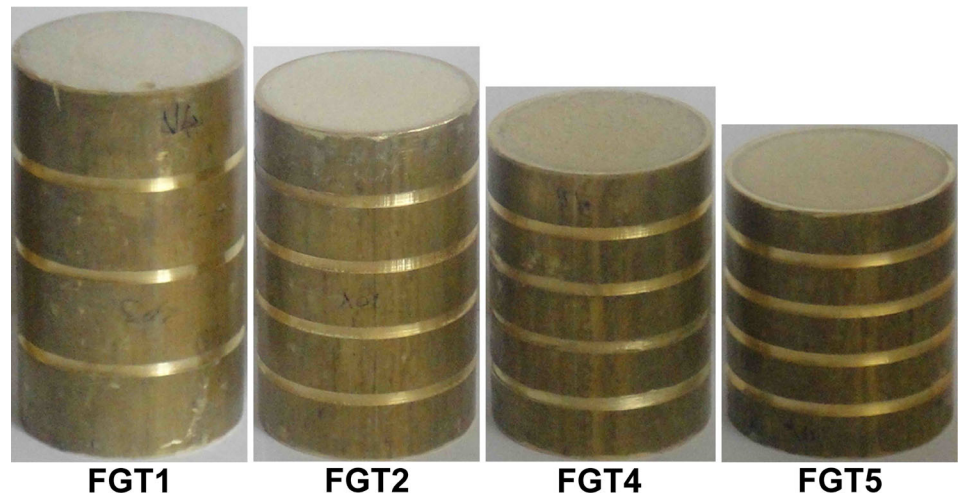


Fig. 7 Experimental and theoretical diagram of the axial force versus the displacement in the empty grooved tube GT1

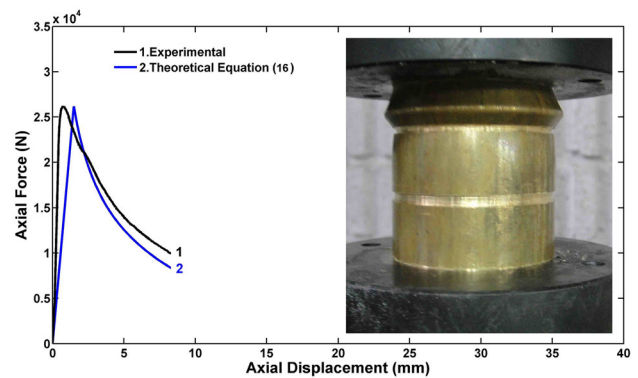


Fig. 9 Experimental and theoretical diagram of the axial force versus the displacement in the empty grooved tube GT3

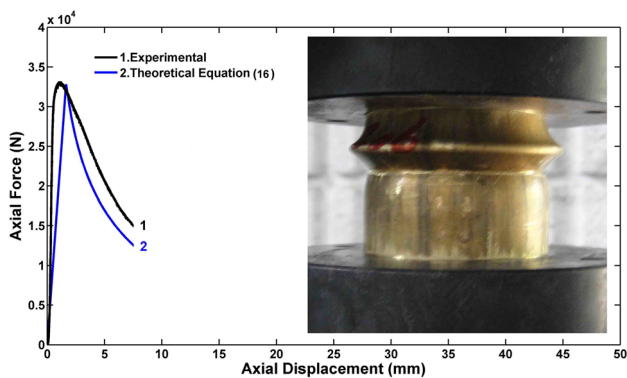


Fig. 8 Experimental and theoretical diagram of the axial force versus the displacement in the empty grooved tube GT2

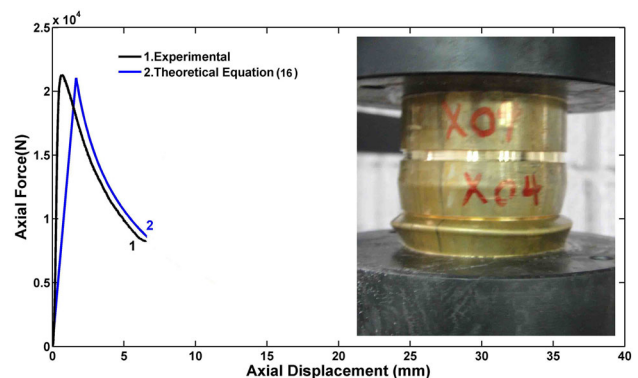


Fig. 10 Experimental and theoretical diagram of the axial force versus the displacement in the empty grooved tube GT4

were assumed in an empty grooved tube: bending around two internal circular hinge lines, bending around an external circular hinge line, and extensional deformation in the folding arms. Comparison of the analytical and

experimental results shows that the assumed deformation modes in the theoretical deformation model is logical and has a good agreement with the plastic deformation in the specimens.

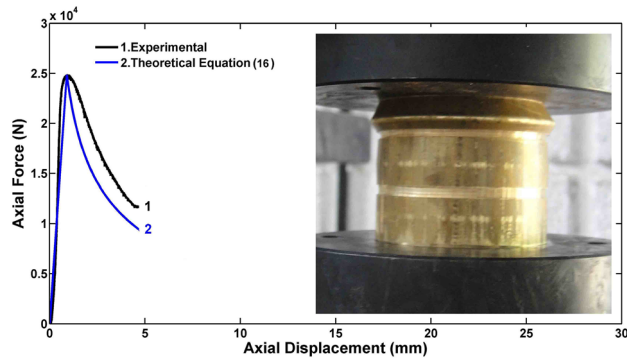


Fig. 11 Experimental and theoretical diagram of the axial force versus the displacement in the empty grooved tube GT5

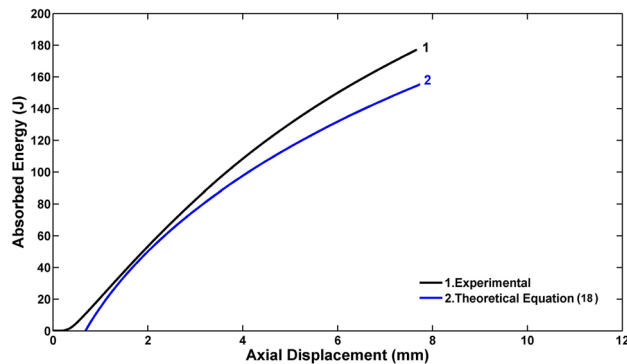


Fig. 12 Experimental and theoretical diagram of the absorbed energy versus the displacement in the empty grooved tube GT2

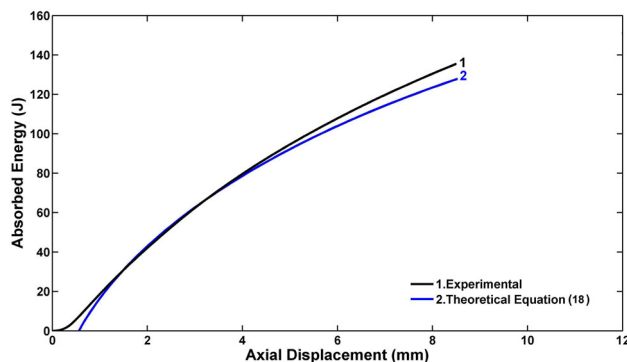


Fig. 13 Experimental and theoretical diagram of the absorbed energy versus the displacement in the empty grooved tube GT3

4.3 Verification of Equations (24) and (25)

Equations (24) and (25) estimate axial load of the foam-filled grooved tubes versus the axial displacement during the first fold creation without and with the interaction effect, respectively. Figures 14, 15, 16, 17, and 18 show comparison of the theoretical and experimental results of the instantaneous folding force in the filled specimens. In

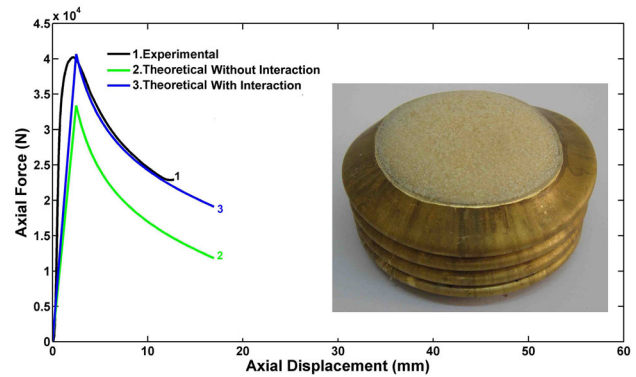


Fig. 14 Experimental and theoretical diagram of the axial force versus the displacement in the foam-filled grooved tube FGT1

the all cases, curve of the axial folding force without considering the interaction effect is less than the corresponding experimental curve with a considerable difference. It results in the interaction effect of tube foam has a remarkable share of the total absorbed energy by a foam-filled grooved tube. During a fold formation, the inner wall moves toward the tube's inside and the foam intercepts. This phenomenon creates the interaction effect between inner wall of the tube and the polyurethane foam, and therefore, the required axial load for compressing the specimen is increased. The mentioned figures show that diagram of the axial load with considering the interaction effect has a better agreement with the experiments, comparing of the theoretical corresponding curve without the interaction effect. It is concluded that the absorbed energy due to the interaction effect of tube foam is as the same as the absorbed energy by the polyurethane foam, and therefore, the interaction effect coefficient is equal to 2.

4.4 Verification of Equations (27) and (28)

Figures 19 and 20 compare the theoretical prediction by Eqs. (27) and (28), respectively, without and with considering the interaction effect with the corresponding experimental measurements. The theoretical predictions without the interaction effect have considerable difference with the experiments, and Eq. (27) always estimates the absorbed energy less than the experiments, but predictions of Eq. (28) with considering the interaction effect have good agreement with the corresponding experiments. Whereas, share of the plastic deformation in the total absorbed energy by the structure is very more than the elastic one, in the theoretical analysis the elastic part was neglected, and just the plastic deformation modes were investigated and calculated. The good correlation between predictions of Eq. (28) and experiments shows verity of the initial assumption in the presented theories.

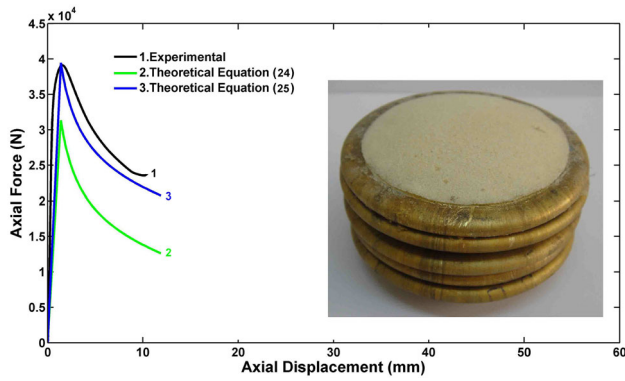


Fig. 15 Experimental and theoretical diagram of the axial force versus the displacement in the foam-filled grooved tube FGT2

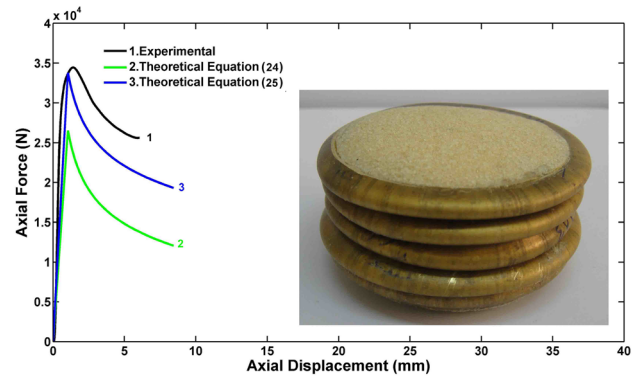


Fig. 18 Experimental and theoretical diagram of the axial force versus the displacement in the foam-filled grooved tube FGT5

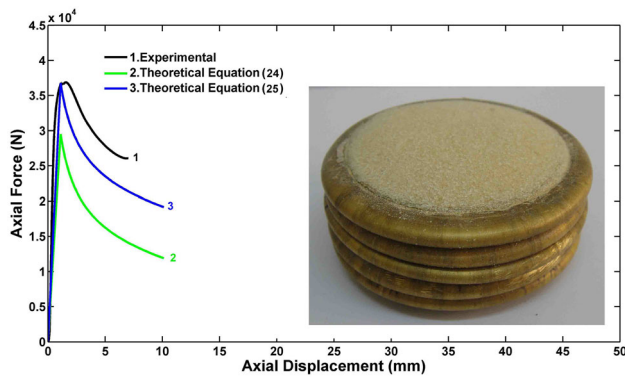


Fig. 16 Experimental and theoretical diagram of the axial force versus the displacement in the foam-filled grooved tube FGT3

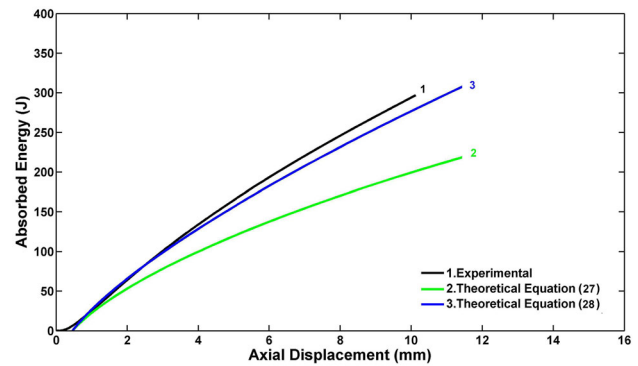


Fig. 19 Experimental and theoretical diagram of the absorbed energy versus the displacement in the foam-filled grooved tube FGT2

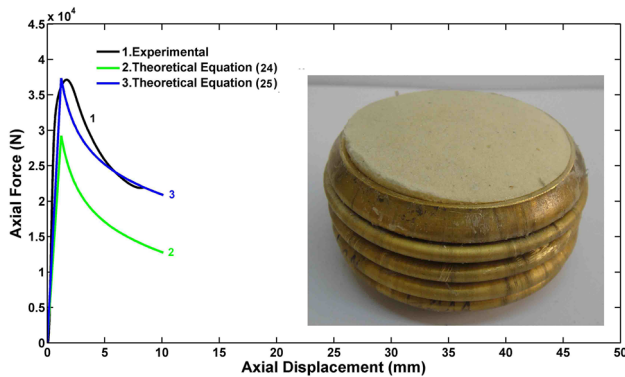


Fig. 17 Experimental and theoretical diagram of the axial force versus the displacement in the foam-filled grooved tube FGT4

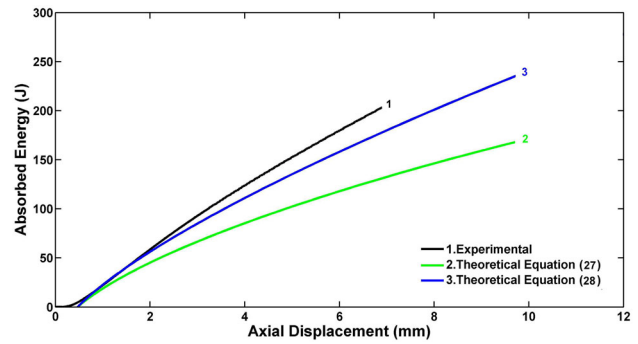


Fig. 20 Experimental and theoretical diagram of the absorbed energy versus the displacement in the foam-filled grooved tube FGT3

4.5 Verification of Equation (30)

Initial length of a BFE is equal to 2λ , and the final length of the BFE after a complete fold formation is equal to $(2\lambda - \Delta_e)$. Δ_e indicates the effective axial displacement. Equation (29) predicts the effective axial displacement, theoretically. But, reviewing of the endpoint of the

theoretical curves in Figs. 14, 15, 16, 17, 18, 19, and 20 and comparison with the corresponding experiments show that estimations of Eq. (29) has a considerable error. Therefore, based on the experimental results of the presented article, the following relation is suggested to predict the effective axial displacement at the end of a complete fold creation in the polyurethane foam-filled grooved tubes, theoretically:

Table 5 Experimental and theoretical results of effective axial displacement

Specimens code	Effective axial displacement (mm)				
	Experiments	Equation (29)	Error percentage of Eq. (29)	Equation (31)	Error percentage of Eq. (31)
FGT1	12.46	17.12	37.42	13.6	9.16
FGT2	10.08	11.96	18.61	9.4	6.78
FGT3	6.85	10.24	49.4	8	16.72
FGT4	8.17	10.24	25.39	8	2.04
FGT5	5.94	8.52	43.5	6.6	11.16

$$\Delta_e = 1.40\lambda - t \quad (31)$$

Table 5 compares the experimental measurement of the effective axial displacement with the theoretical predictions by Eqs. (29) and (31) and the error percentages. In Table 5, results show that the semi-empirical relation (31) predict the effective axial displacement with more accuracy than the theoretical relation (29).

Figure 2 illustrates a foam-filled grooved tube before the axial compression. Also, real mechanical behavior and theoretical deformation model of the filled grooved tube have been illustrated in the figure. In reality, during the fold creation, a part of tube wall that is a straight line between two contiguous inside and outside grooves, rotates and transforms into a curve. However, in the theoretical deformation model, rotation of the tube wall around the plastic hinge lines has been considered, but the recent mentioned curvature of tube wall was not considered in the theory. Also, during the fold creation, folded tube walls reach to each other and the friction phenomenon occurs between them, while the effects of this phenomenon were not considered in the theoretical model. In addition, generally, Poisson ratio of the polyurethane foam is very small, but it is not exactly equal to zero; whereas, in the derived theory of the present paper, Poisson ratio of the foam was considered equal to zero and barreling phenomenon has been neglected. The above reasons justify the considered differences between the theoretical and experimental results.

5 Conclusion

In this paper, some theoretical relationship were derived to predict the instantaneous folding force and absorbed energy during the first fold creation in the empty and polyurethane foam-filled circular grooved tubes. For this purpose, the dissipated energy rates by empty and filled circular grooved tubes were considered consist of bending energy rate in plastic hinge lines, extensional energy rate, energy of foam deformation, and interaction effect between the inner wall of the tube and lateral surface of

polyurethane foam. Also, the effective axial displacement was calculated to predict the endpoint of axial displacement in the first fold creation, semi-empirically. Comparison of the experimental results and theoretical predictions shows a good correlation.

References

- Abedi MM, Niknejad A, Liaghat GH, Zamani Nejad M (2012) Theoretical and experimental study on empty and foam-filled columns with square and rectangular cross section under axial compression. *Int J Mech Sci* 65:134–146
- Adachi T, Tomiyamal A, Araki W, Yamaji A (2008) Energy absorption of a thin-walled cylinder with ribs subjected to axial impact. *Int J Impact Eng* 35:65–79
- Bardi FC, Kyriakides S (2006) Plastic buckling of circular tubes under axial compression—part I: experiments. *Int J Mech Sci* 48:830–841
- Bardi FC, Yun HD, Kyriakides S (2003) On the axisymmetric progressive crushing of circular tubes under axial compression. *Int J Solids Struct* 40:3137–3155
- Daneshi GH, Hosseinipour SJ (2002) Elastic-plastic theory for initial buckling load of thin-walled grooved tubes under axial compression. *J Mater Process Technol* 125–126:826–832
- Guden M, Kavi H (2006) Quasi-static axial compression behavior of constraint hexagonal and square-packed empty and aluminum foam-filled aluminum multi-tubes. *Thin Walled Struct* 44:739–750
- Lee KS, Kim SK, Yang IY (2008) The energy absorption control characteristics of Al thin-walled tube under quasi-static axial compression. *J Mater Process Technol* 201:445–449
- Li Z, Yu J, Guo L (2012) Deformation and energy absorption of aluminum foam-filled tubes subjected to oblique loading. *Int J Mech Sci* 54:48–56
- Nakamoto H, Adachi T, Araki W (2009) In-plane impact behavior of honeycomb structures filled with linearly arranged inclusions. *Int J Impact Eng* 36:1019–1026
- Niknejad A, Tavassolimanesh A (2013) Axial compression of the empty capped-end frusta during the inversion progress. *Mater Des* 49:65–75
- Niknejad A, Liaghat GH, Moslemi Naeini H, Behraves AH (2010) Experimental and theoretical investigation of the first fold creation in thin walled columns. *Acta Mech Solida Sin* 23:353–360
- Niknejad A, Liaghat GH, Moslemi Naeini H, Behraves AH (2011) Theoretical and experimental studies of the instantaneous folding force of the polyurethane foam-filled square honeycombs. *Mater Des* 32:69–75

- Niknejad A, Elahi SA, Liaghat GH (2012a) Experimental investigation on the lateral compression in the foam-filled circular tubes. *Mater Des* 36:24–34
- Niknejad A, Abedi MM, Liaghat GH, Zamani Nejad M (2012b) Prediction of the mean folding force during the axial compression in foam-filled grooved tubes by theoretical analysis. *Mater Des* 37:144–151
- Niknejad A, Rezaei B, Liaghat GH (2013) Empty circular metal tubes in the splitting process theoretical and experimental studies. *Thin Walled Struct* 72:48–60
- Niknejad A, Abedi MM, Liaghat GH, Zamani Nejad M (2015) Absorbed energy by foam-filled quadrangle tubes during the crushing process by considering the interaction effects. *Arch Civ Mech Eng* 15:376–391
- Park C, Nutt SR (2002) Strain rate sensitivity and defects in steel foam. *Mater Sci Eng, A* 323:358–366
- Santosa SP, Wierzbicki T, Hanssen AG, Langseth M (2000) Experimental and numerical studies of foam-filled sections. *Int J Impact Eng* 24:509–534
- Savage G, Bomphray I, Oxley M (2004) Exploiting the fracture properties of carbon fibre composites to design lightweight energy absorbing structures. *Eng Fail Anal* 11:677–694
- Tan PJ, Reid SR, Harrigan JJ, Zou Z, Li S (2005) Dynamic compressive strength properties of aluminium foams. Part II—shock theory and comparison with experimental data and numerical models. *J Mech Phys Solids* 53:2206–2230
- Tasdemirci A (2008) The effect of tube end constraining on the axial crushing behavior of an aluminum tube. *Mater Des* 29:1992–2001
- Tyagi BL, Abbas H, Arif M, Gupta NK (2004) Change in thickness in curved fold model for axial crushing of tubes. *Int J Solids Struct* 41:7129–7153
- Wang Z, Shen J, Lu G, Zhao L (2011) Compressive behavior of closed-cell aluminum alloy foams at medium strain rates. *Mater Sci Eng, A* 528:2326–2330
- Zhang X, Huh H (2009) Energy absorption of longitudinally grooved square tubes under axial compression. *Thin Walled Struct* 47:1469–1477
- Zou Z, Reid SR, Tan PJ, Li S, Harrigan JJ (2009) Dynamic crushing of honeycombs and features of shock fronts. *Int J Impact Eng* 36:165–176